

## Original Paper

### Domain Structure of Misfit-layered Compounds in Bi-Ca-Co-O

Kunio YUBUTA<sup>1,2,\*</sup>, Shahnaz BEGUM<sup>2,3</sup>, Yasuhiro ONO<sup>2,3</sup>, Yuzuru MIYAZAKI<sup>2,3</sup>, Tsuyoshi KAJITANI<sup>2,3</sup>

<sup>1</sup>Institute for Materials Research, Tohoku University, Sendai 980-8577

<sup>2</sup>Core Research for Evolutional Science and Technology, Japan Science and Technology Agency, Tokyo 103-0027

<sup>3</sup>Department of Applied Physics, Graduate School of Engineering, Tohoku University, Sendai 980-8579

Received January 10, 2008; E-mail: yubuta@imr.tohoku.ac.jp

The domain structure of  $\text{Bi}_{1.84}\text{Ca}_{2.00}\text{Co}_{1.88}\text{O}_x$  is studied by electron diffraction analysis and high-resolution electron microscopy. The crystal structure consists of two interpenetrating monoclinic subsystems of a triangular  $\text{CoO}_2$  sheet and a distorted four-layered  $\text{Bi}_2\text{Ca}_2\text{O}_4$  rock-salt (RS)-type block layers. Both subsystems have common  $a$ -,  $c$ -axes and  $\beta$ -angle with  $a = 4.90 \text{ \AA}$ ,  $c = 14.36 \text{ \AA}$ , and  $\beta = 93.0^\circ$ . On the other hand, the crystal structure is incommensurately modulated parallel to the  $b$ -axes, in which  $b_1 = 2.79 \text{ \AA}$  for the  $\text{CoO}_2$  sheet and  $b_2 = 4.78 \text{ \AA}$  for the  $\text{Bi}_2\text{Ca}_2\text{O}_4$  RS-type block layers, respectively. These vectors characterize the structure analogue as  $[(\text{Bi}_{1.84}\text{Co}_{0.16})\text{Ca}_{2.00}\text{O}_y]_{0.58}[\text{CoO}_2]$  being Bi-poor relative to Ca. This compound has two modulation vectors, namely,  $\mathbf{q}_1 = -\mathbf{a}^* + 0.58\mathbf{b}_1^*$  and  $\mathbf{q}_2 = 0.18\mathbf{b}_1^* + 0.5\mathbf{c}^*$ . Both modulation vectors are different from the ones in  $[\text{Bi}_{0.87}\text{SrO}_2]_2[\text{CoO}_2]_{1.82}$  studied by Leligny *et al.* [Acta Crystallogr. B, **2000**, *56*, 173]. High-resolution images taken with the incident electron beam parallel to the  $a$ - and  $c$ -axes clearly exhibit modulated atomic arrangements. Diffuse streaks are observed in the  $a^*-b^*$  plane in the present system. The local modulation mode characterized by the diffuse scattering is related to the domain structure in the  $a$ - $b$  plane.

Key Words: *Thermoelectric Compound, Misfit-Layered Structure, Modulated Structure, Residual Strain, Electron Diffraction, High-Resolution Image*

#### 1. Introduction

Since the discovery of a large thermopower in  $\text{Bi}_{2.3-x}\text{Pb}_x\text{Sr}_{2.6}\text{Co}_2\text{O}_y$  ( $0 \leq x \leq 0.44$ )[1], because of composite structure and high thermoelectric performances, the misfit-layered Bi-based cobaltites have accumulated many researchers' attention[2-6].  $\text{Bi}-\text{Sr}-\text{Co}-\text{O}$ [7,8] and  $\text{Bi}-\text{Ca}-\text{Co}-\text{O}$ [9-12] crystals were elucidated and it was found that they consist of edge-sharing triangular  $\text{CoO}_2$  sheets and four-layered  $\text{Bi}_2(\text{Sr},\text{Ca})_2\text{O}_4$  RS-type block layers interpenetrating alternately in the  $c$ -axis direction, as shown in Fig.1. These two subsystems are incommensurately interpenetrating parallel to the  $b$ -axis. In some cases, additional intrinsic modulations were observed.

Streak intensities are frequently observed parallel to the  $[110]^*$  in the  $a^*-b^*$  plane of the misfit layered Bi-oxides[4,13]. Recently, we directly observed the shear-displacement-type modulation in  $[\text{Bi}_{1.69}\text{Ba}_{1.88}\text{O}_y]_{0.56}[\text{RhO}_2]$ [14] and  $[\text{Bi}_{2.08}\text{Sr}_{1.67}\text{O}_y]_{0.54}[\text{CoO}_2]$ [15] by means of the high-resolution transmission electron microscopy (HREM). The diagonal-type modulation in the  $a^*-b^*$  plane has been observed with local shear-type structural deformation, which causes local discontinuity, i.e., a kind of discommensuration in the  $a$ - $b$  plane.

To understand local crystal structure in the  $\text{Bi}-\text{Ca}-\text{Co}-\text{O}$  system, we have employed the high-resolution microscopy techniques. The present study is carried out according to the (3+2)-dimensional superspace group approach[8,11,14-18].

#### 2. Experimental details

Polycrystalline samples were prepared by the standard solid-state reaction method.  $\text{Bi}_2\text{O}_3$ ,  $\text{CaCO}_3$  and  $\text{Co}_3\text{O}_4$  powders weighed in the molar ratio at  $\text{Bi}:\text{Ca}:\text{Co} = 31:32:37$  (sample A) and  $\text{Bi}:\text{Ca}:\text{Co} = 31:34:35$  (sample B), were mixed in an agate mortar and pressed into pellets. The pellets were heated at  $800^\circ\text{C}$  for 12 h in air. Then,

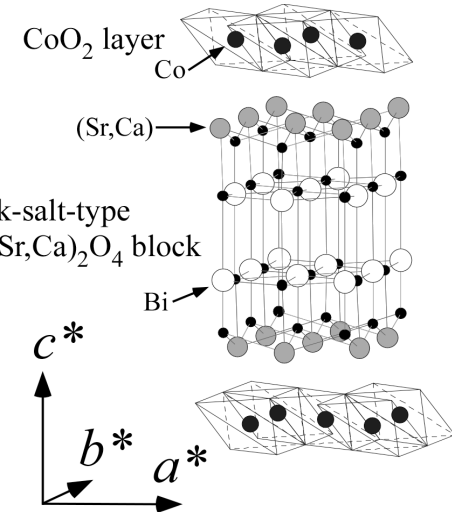


Fig.1 Schematic illustration of crystal structure of the misfit layered  $\text{Bi}-(\text{Sr},\text{Ca})-\text{Co}-\text{O}$  compounds.

the samples were furnace-cooled to room temperature. After grinding, the powders were pelletized and heated at  $840^\circ\text{C}$  for 12 h in air followed by furnace cooling. It was confirmed that the secondary phase was not formed by means of X-ray powder diffraction measurement.

Chemical analysis was carried out with the backscattered electron images, using an electron probe microanalyzer (EPMA;

JEOL JXA-8621MX). An averaged composition was obtained from more than five different parts of the samples. Chemical compositions are listed in Table 1. The Bi content is significantly lower than Ca content in either case. The deficiencies of Bi is rather commonly seen in the Bi-Ca-Co-O system such as  $[Bi_{1.7}Co_{0.3}Ca_2O_4]^{RS}[CoO_2]_{1.67}$ [9]. On the other hand, an exceptional case was also reported by Guilmeau *et al.* insisting that the Bi/Ca ratio is almost unity in  $[BiCaO_2]_2[CoO_2]_{1.69}$ [12].

Electron diffraction patterns and HREM images were obtained using a 200 kV electron microscope (JEM-2010) at a resolution of 1.9 Å.

Table 1 Nominal and analytical compositions.

Bi : Ca : Co	Sample A	Sample B
Nominal compositions	1.94 : 2.00 : 2.31	1.82 : 2.00 : 2.06
Analytical compositions	1.70 : 2.00 : 1.93	1.84 : 2.00 : 1.88

### 3. Results and Discussion

#### 3.1 Electron diffraction patterns

Figures 2(a)-2(h) show electron diffraction patterns of Bi-Ca-Co-O samples A and B taken with the incident beam parallel to the four principal axes. Figures 2(a), 2(c), 2(e) and 2(g), i.e., the left column, are obtained from the sample A. The rest of the diffraction patterns in the right column are obtained from the sample B. From the obtained diffraction patterns, it is clear that the both compounds have a composite structure consisting of two monoclinic subsystems. One can recognize that the two unit cells have common  $a$ - and  $c$ -axes and mutually incommensurated  $b_1$ - and  $b_2$ -axes, one of the characteristic features of the misfit-layered structure.

The construction of the reciprocal lattice was studied by tilting around the crystalline axes. The estimated four axis lengths and  $\beta$ -angles were listed in Table 2. We assigned the  $CoO_2$  sheet,  $CdI_2$ -type layers, to be subsystem 1 and the  $Bi_2Ca_2O_4$  RS-type block layers to be subsystem 2. Four integers  $h$ ,  $k$ ,  $l$  and  $m$  are necessary to index the fundamental electron diffraction spots. The reciprocal lattice vector  $\mathbf{g}$  can be expressed using four indices as  $\mathbf{g} = ha^* + kb_1^* + lc^* + mb_2^*$ .  $S^*$  shown in Figs.2(a), 2(b), 2(g) and 2(h) represents the  $[100\bar{1}]$  direction. Some deficiencies at the Bi site are assumed on the basis of the determined metal ratio by EPMA, i.e.,  $Bi:Ca:Co = 1.70:2.00:1.93$  for sample A and  $Bi:Ca:Co = 1.84:2.00:1.88$  for sample B. The axial ratios of  $b_1/b_2 \sim 0.61$  (sample A) and 0.58 (sample B) give the structure analogues as  $[(Bi_{1.70}Co_{0.30})Ca_{2.00}O_y]_{0.61}[CoO_2]$  and  $[(Bi_{1.84}Co_{0.16})Ca_{2.00}O_y]_{0.58}[CoO_2]$ , respectively. The misfit ratios of the misfit compounds in this study at about 0.60, are very close to those of  $[Bi_{1.7}Co_{0.3}Ca_2O_4]^{RS}[CoO_2]_{1.67}$ [9] and  $[BiCaO_2]_2[CoO_2]_{1.69}$ [12] having the misfit ratios at  $1/1.67 = 0.60$  and  $1/1.69 = 0.59$ , respectively.

Table 2 Lattice parameters and misfit ratios.

	Sample A	Sample B
$a$ (Å)	4.94	4.90
$b_1$ (Å)	2.83	2.79
$b_2$ (Å)	4.62	4.78
$c$ (Å)	14.64	14.36
$\beta$ (°)	93.6	93.0
$b_1/b_2$	0.61	0.58

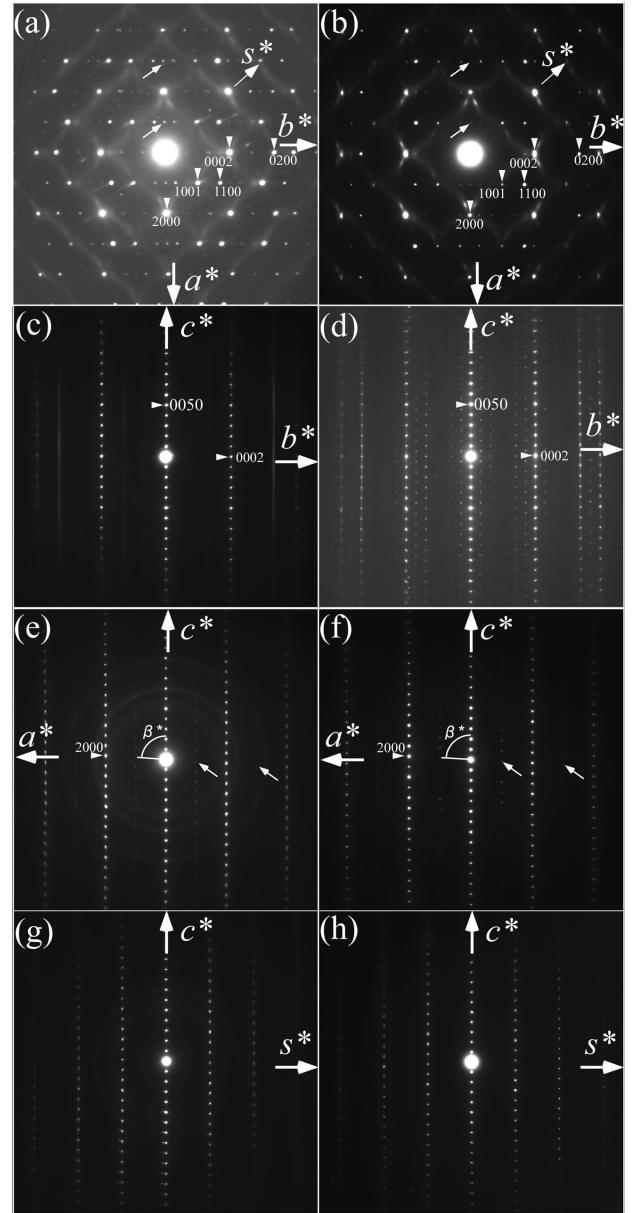


Fig.2 Electron diffraction patterns (a, c, e, g) of  $[(Bi_{1.70}Co_{0.30})Ca_{2.00}O_y]_{0.61}[CoO_2]$  and (b, d, f, h) of  $[(Bi_{1.84}Co_{0.16})Ca_{2.00}O_y]_{0.58}[CoO_2]$  taken with the incident electron beam parallel to [0010] for panels (a, b), [1000] for (c, d), [0101] for (e, f) and [1001] for (g, h), respectively.

In Figs.2(a) and 2(b), small arrows indicate  $h000$  ( $h=odd$ ) weak reflections which are also seen in Figs.2(e) and 2(f). These spots evidence the breaking down of the  $C$ -centered symmetry. We could obtain the following reflection conditions for samples A and B as:  $k = 2n$  for the  $0k00$  reflections and  $m = 2n'$  for the  $000m$  reflections, implying that the possible space groups of the two samples are  $P2_1$  or  $P2_1/m$ -types[19]. We, hereafter, assume centrosymmetric  $P2_1/m$ -type unit cells, having the higher symmetry than  $P2_1$ , for the present structure analysis. It is exhibited that this symmetry is not identical with that of  $[Bi_{0.87}SrO_2]_2[CoO_2]_{1.82}$ [8], which is a Bi-poor phase. On the other hand, this symmetry-type,  $P2_1/m$ , is identical with that of  $[Bi_{2.08}Sr_{1.67}O_y]_{0.54}[CoO_2]$ [15], which is a Bi-rich phase.

The characteristic features of the diffraction patterns in Figs.2(a) and 2(b) are the streaks running parallel either to  $[1001]^*$  and  $[100\bar{1}]^*$ . Similar streaks were observed in  $Bi_2M_3Co_2O_y$  ( $M = Sr, Ba$ )[20],  $Bi_{2-x}Pb_xSr_2Co_2O_y$ [4],  $[Bi_2Ba_{1.8}Co_{0.2}O_4]^{RS}[CoO_2]_2$ [13],  $[Bi_{1.69}Ba_{1.88}$

$O_y]_{0.56}[RhO_2]$ [14] and  $[Bi_{2.08}Sr_{1.67}O_y]_{0.54}[CoO_2]$ [15]. Hervieu *et al.* concluded that the two-dimensional modulation which was

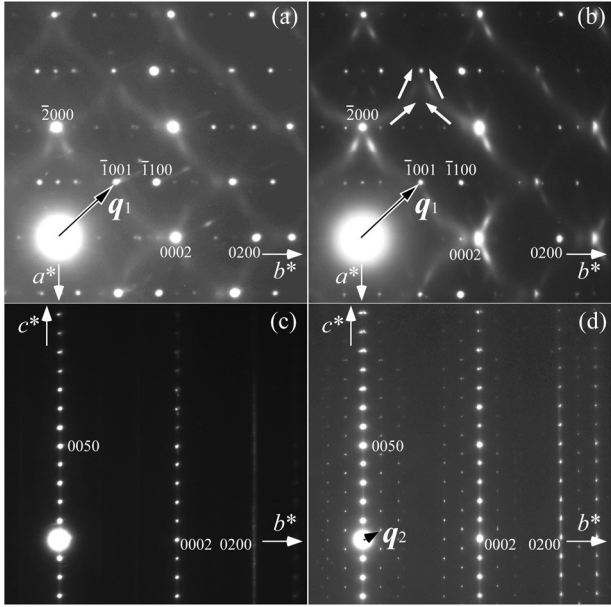


Fig.3 Enlarged electron diffraction patterns (a)-(d) of Fig.2(a)-(d), respectively.

responsible for the streaks presented in  $[Bi_2Ba_{1.8}Co_{0.2}O_4]$  block[13]. We have observed such structural modulation in  $[Bi_{1.69}Ba_{1.88}O_y]_{0.56}[RhO_2]$  and  $[Bi_{2.08}Sr_{1.67}O_y]_{0.54}[CoO_2]$  in the  $a$ - $b$  plane by HREM study.

There are satellite reflections in Figs.2(a), 2(b) and 2(d) but no satellite reflection is seen in Figs.2(c) and 2(e)-2(h). Figures 3(a)-3(d) show enlarged parts of Figs. 2(a)-2(d), respectively. The modulation vectors  $q_1$  are indicated by large arrows in Figs.3(a) and 3(b) and the vector  $q_2$  is indicated by small arrow in Fig.3(d), respectively. In Fig.3(d), satellite reflections are observed only in the vicinity of the fundamental reflections. On the other hand, in Fig. 3(c), no satellite reflection is observed in the vicinity of the  $c^*$ -axis, as similarly reported in the previous study [11]. The origin of  $q_1$  is in the difference of two  $b$ -axis lengths of the two subsystems but  $q_2$  is originated from the intrinsic modulation in the RS-type block. Modulation vectors can be indicated as  $q_1 = -a^* + 0.61b_1^*$  in the sample A but  $q_1 = -a^* + 0.58b_1^*$  and  $q_2 = 0.18b_1^* + 0.5c^*$  in the sample B. Because of number of the modulation vectors,  $[(Bi_{1.70}Co_{0.30})Ca_{2.00}O_y]_{0.61}[CoO_2]$  (sample A) and  $[(Bi_{1.84}Co_{0.16})Ca_{2.00}O_y]_{0.58}[CoO_2]$  (sample B) are regard as (3+1)- and (3+2)-dimensional crystal, respectively.

In  $[Bi_{0.87}SrO_2]_2[CoO_2]_{1.82}$ , Leligny *et al.*[8] concluded that an intrinsic modulation vector was  $q_{11} = 0.293a^* + 0.915c^*$  being different from the vectors  $q_1$  and  $q_2$  defined above. This difference could be due partly to the difference in the ionic radii of  $Ca^{2+}$ ,  $r_{S-P} = 1.00 \text{ \AA}$  and  $Sr^{2+}$ ,  $r_{S-P} = 1.16 \text{ \AA}$  and that of ionic radii due to the substitution of Bi-Co ions. The suffix S-P refers to Shannon-Prewitt radii. Compared with the other modulation vectors, the present  $q_2$  of the sample B have two important characteristics. First,

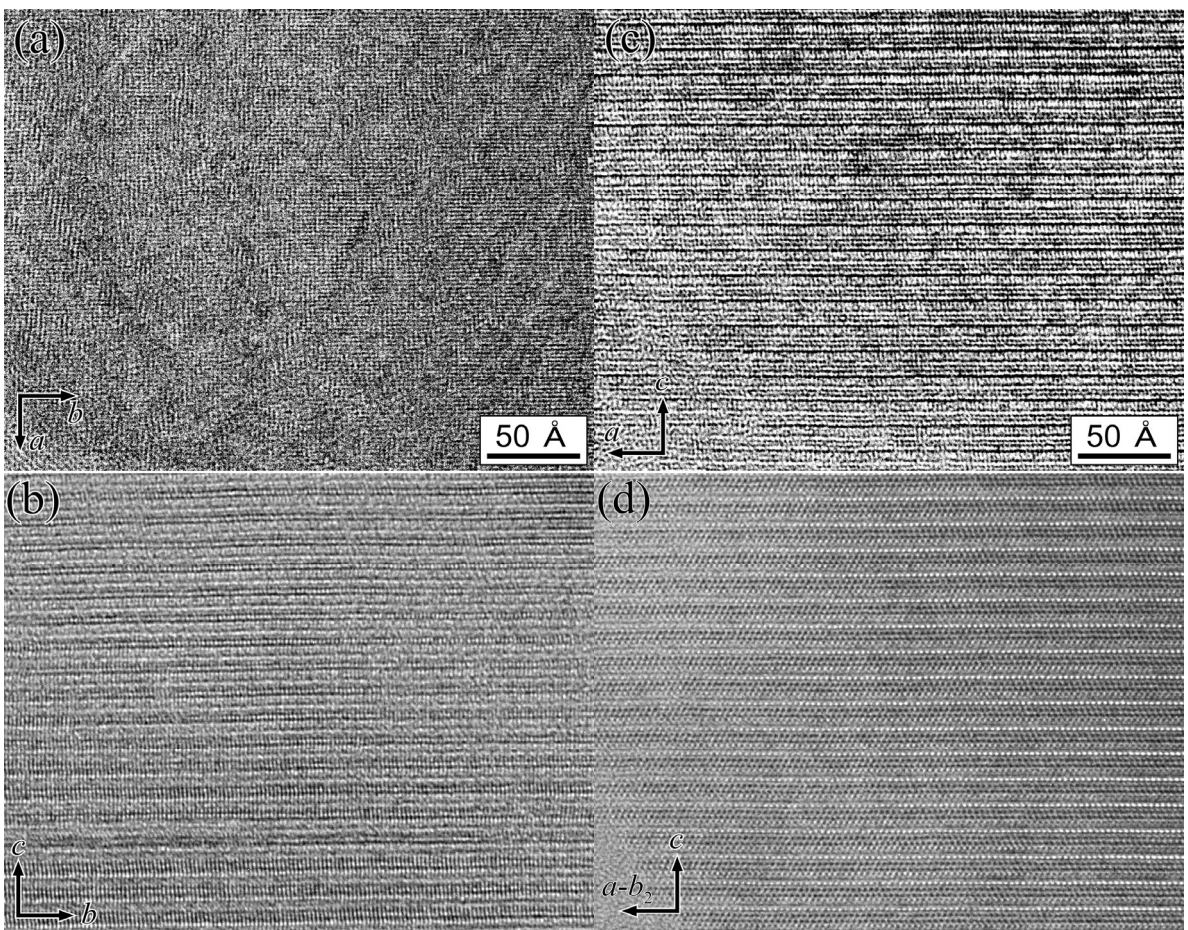


Fig.4 High-resolution electron micrographs taken with the incident beam parallel to [0010] in the panel (a), [1000] in (b), [0101] in (c) and [1001] in (d) of  $[(Bi_{1.84}Co_{0.16})Ca_{2.00}O_y]_{0.58}[CoO_2]$  (sample B).

$\mathbf{q}_2$  exists on the  $b^*-c^*$  plane in  $[(\text{Bi}_{1.84}\text{Co}_{0.16})\text{Ca}_{2.00}\text{O}_y]_{0.58}[\text{CoO}_2]$ , whereas  $\mathbf{q}_{11}$  exists on the  $a^*-c^*$  plane in  $[\text{Bi}_{0.87}\text{SrO}_2]_2[\text{CoO}_2]_{1.82}$ . Second, the  $c^*$  component of  $\mathbf{q}_2$  is rational, i.e., 0.5, in the present  $[(\text{Bi}_{1.84}\text{Co}_{0.16})\text{Ca}_{2.00}\text{O}_y]_{0.58}[\text{CoO}_2]$ .

In Fig. 3(b), diffuse streaks exist between Bragg reflections. Another type of diffuse intensities is also noticed in the four directions, as indicated by white arrows. Similar additional modulation modes characterized by the vectors  $\mathbf{q}_i = 0.2(a_{\text{RS}}^* + b_{\text{RS}}^*)$ ,  $\mathbf{q}_3 = -0.12\mathbf{a}^* + 0.10\mathbf{b}_1^*$  and  $\mathbf{q}_3 = -0.14\mathbf{a}^* + 0.10\mathbf{b}_1^*$  have already been assigned in  $[\text{Bi}_2\text{Ba}_{1.8}\text{Co}_{0.2}\text{O}_4]^{\text{RS}}[\text{CoO}_2]_2$ [13],  $[\text{Bi}_{1.69}\text{Ba}_{1.88}\text{O}_y]_{0.56}[\text{RhO}_2]$ [14] and  $[\text{Bi}_{2.08}\text{Sr}_{1.67}\text{O}_y]_{0.54}[\text{CoO}_2]$ [15], respectively. Asymmetric diffuse intensity distribution is found in the vicinities of fundamental reciprocal lattice points. The asymmetric and streaky nature of the diffuse reflections suggests that the new modulation mode (four-types) is associated with shear-displacement-type modulation. This point will be confirmed from HREM images in Figs.4, 5 and 6 later. Samples A and B have similar crystal structures but the vector  $\mathbf{q}_2$  exist only in the sample B. Hereafter, we will discuss modulated crystal structure of sample B which is regarded as a modulated structure of sample A with the vector  $\mathbf{q}_2$ .

### 3.2 HREM images of $[(\text{Bi}_{1.84}\text{Co}_{0.16})\text{Ca}_{2.00}\text{O}_y]_{0.58}[\text{CoO}_2]$

Figures 4(a)-4(d) show high-resolution electron micrographs of

$[(\text{Bi}_{1.84}\text{Co}_{0.16})\text{Ca}_{2.00}\text{O}_y]_{0.58}[\text{CoO}_2]$ , i.e., the sample B, corresponding to the electron diffraction patterns in Figs.2(b), 2(d), 2(f) and 2(h), respectively. It can be easily seen that the sample crystal consists of following sequence of  $MO_x$  layers, namely,  $\text{BiO}-\text{BiO}-\text{CaO}-\text{CoO}_2-\text{CaO}-\text{BiO}-\text{BiO}\dots$ , parallel to the  $c$ -direction.

Together with the crossed lattice fringes, a noticeable modulation of image contrast can be observed in Fig.4(a). But stacking faults fringes parallel to the [1001] direction were not observed, in contrast to  $[\text{Bi}_{1.69}\text{Ba}_{1.88}\text{O}_y]_{0.56}[\text{RhO}_2]$ [14] and  $[\text{Bi}_{2.08}\text{Sr}_{1.67}\text{O}_y]_{0.54}[\text{CoO}_2]$ [15]. Since diffuse scattering, running along the <1001>, is weak, the image contrast in the  $a-b$  plane is not strongly disturbed.

Figure 4(b) exhibits a typical modulated structure, being curved locally and has close similarity to those of the high- $T_c$  superconductor  $\text{Bi-Pb-Sr-Ca-Cu-O}$ [21-23] and its related compounds[24,25]. In addition, the image contrast of the RS-type blocks, parallel to the  $b_2$ -axis, is not uniform. Figure 4(b) shows a sequential lattice expansion and contraction in the bright and dark regions, respectively, although, one can recognize unmodulated layered structures in Figs.4(c) and 4(d).

To observe atomic arrangements clearly, image processing, i.e., Fourier filtering, was employed. Figures 5(a)-5(d) represent the reconstructed images of Figs.4(a)-4(d), respectively, by the Fourier synthesis procedure using Fast Fourier Transform (FFT). Fourier

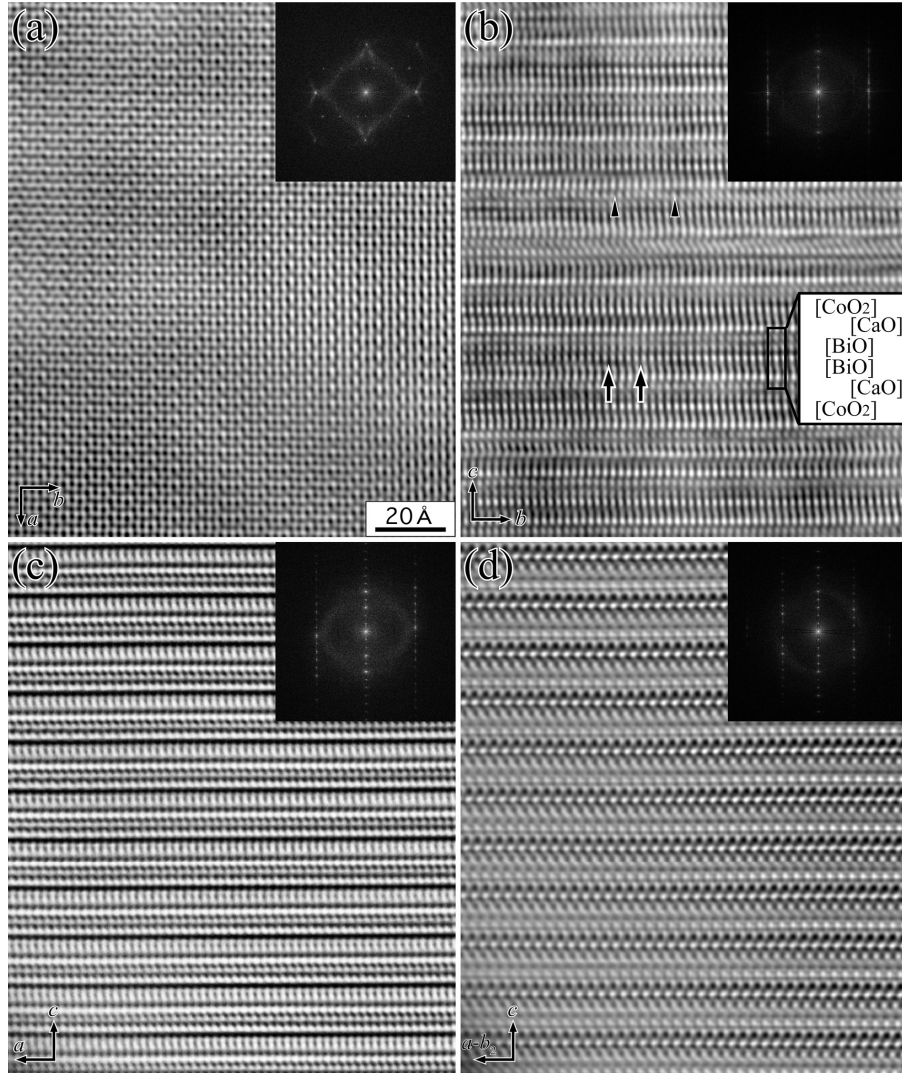


Fig.5 Fourier-filtered HREM images taken with the incident electron beam parallel to [0010] in the panel (a), [1000] in (b), [0101] in (c) and [1001] in (d). The insets show the power spectra of images in Figs.4, respectively.

synthesis calculation was carried out using (a)  $hk0m$  reflections, (b)  $0klm$  ones with satellite ones, (c)  $h0l0$  ones and (d)  $h0lh$  ones, respectively. Each inset shows the power spectra of HREM image in Figs.4. The atomic arrangements projected to the [1001] and [ $\bar{1}$  001] directions seem perfectly ordered in Fig.5(a). Contrast modulation was observed in Fig.5(b). Especially, it can be seen in BiO layers in RS-type blocks as indicated by arrows. It is suggested that the modulation evidences the partial Co substitutions for Bi-deficiency sites. The arrowheads exhibit a long periodicity, at about 16 Å, corresponding to the modulation vector  $q_2$  in Fig.5(b). On the other hand, one cannot recognize any long-period contrast and/or structural modulation in Figs.5(c) and 5(d).

### 3.3 Diffuse scattering and residual strain model

Figure 6 represents the FFT filtered image of Fig.4(a) using only streak intensities shown in the inset. Characteristic shear-type discontinuity lines are clearly observed at the positions indicated by arrowheads. These discontinuity lines have close correspondence with the structural modulation mode characterized by the four vectors in Fig.3(b). Also this crystal has a kind of domain structure. Each domain has four different shearing deformation directions. The size of domains is approximately 50–100 Å in the <1001> directions. In the stripe ranges seen between two discontinuity lines, the image contrast is slightly bright and disturbed. It is conceivable that the origin of the structural modulations in the  $a$ - $b$  plane is identical with those of  $[Bi_{1.69}Ba_{1.88}O_y]_{0.56}[RhO_2]$  and  $[Bi_{2.08}Sr_{1.67}O_y]_{0.54}[CoO_2]$ .

In above systems, CdI<sub>2</sub>-type layers and RS-type blocks are found to be mutually strained, nearly two dimensionally, i.e.,

$$e_{11} = \left\{ a - \left( \frac{a+b_2}{2} \right) \right\} / \frac{a+b_2}{2} = -e_{22}$$

where  $e_{ij}$  is the strain tensor element. For our simplicity, assume two-dimensional residual strain, for which  $e_{11} = -e_{22}$  and  $e_{12} = e_{21} = 0$ , in the  $a$ - $b$  planes of the RS-type blocks and CdI<sub>2</sub>-type layers. Bi-M(Co, Rh)-O system with  $M = Ba$  or  $Sr$ , are typical misfit-layered

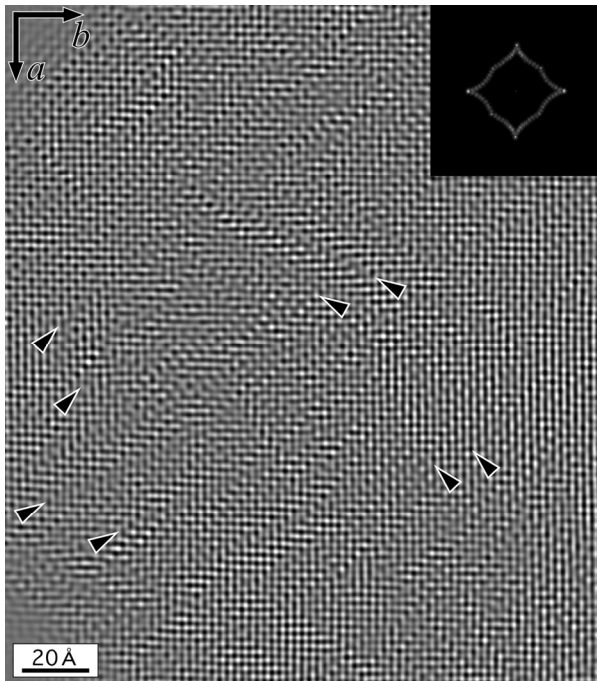


Fig.6 A Fourier-filtered HREM image using diffuse scatterings of Fig.4(a). The inset shows the distribution of the power spectrum used in Fourier-transformation. Four-direction-type domains are indicated by arrowheads.

Table 3 Strain tensor elements of RS-type blocks,  $e_{11}$ .

	Strain tensor element
	$e_{11}$
$[Bi_{1.84}Co_{0.16}]Ca_{2.00}O_y]_{0.58}[CoO_2]$	0.0124
$[Bi_{1.94}Ba_{1.83}O_y]_{0.56}[RhO_2]$ <sup>[15]</sup>	-0.0065
$[Bi_{1.79}Sr_{1.98}O_y]_{0.63}[RhO_2]$ <sup>[17]</sup>	0.0394
$[Bi_{2.08}Sr_{1.67}O_y]_{0.54}[CoO_2]$ <sup>[16]</sup>	-0.0167

ones which have BiO double layers as in the present system. In Table 3, the strain tensor elements of RS-type blocks are listed. There are significant difference in deformation-type between  $[Bi_2Ba_{1.8}Co_{0.2}O_4]^{RS}[CoO_2]_2$  and  $[Bi_{2.08}Sr_{1.67}O_y]_{0.54}[CoO_2]$ , which have [1001]-type modulations in the  $a^*-b^*$  plane and  $[(Bi_{1.84}Co_{0.16})Ca_{2.00}O_y]_{0.58}[CoO_2]$ , which have [1001]- and [1001]-type ones. That is,  $e_{11}$  is less than 0 in  $[Bi_2Ba_{1.8}Co_{0.2}O_4]^{RS}[CoO_2]_2$  and  $[Bi_{2.08}Sr_{1.67}O_y]_{0.54}[CoO_2]$ . On the other hand,  $e_{11}$  is greater than 0 in  $[(Bi_{1.84}Co_{0.16})Ca_{2.00}O_y]_{0.58}[CoO_2]$ .

In the present crystal,  $[(Bi_{1.84}Co_{0.16})Ca_{2.00}O_y]_{0.58}[CoO_2]$ , it is found  $e_{11} = -e_{22} = +0.0124$ , i.e., the RS-type layers are expanded and compressed parallel to the  $a$ - and  $b_2$ -axes, respectively. Figures 7(a) and 7(b) show schematic illustrations of the  $a$ - $b$  real lattice planes in  $[(Bi_{1.84}Co_{0.16})Ca_{2.00}O_y]_{0.58}[CoO_2]$ . The RS-type block in Fig.7(a) is expanded and compressed parallel to the  $a$ - and  $b$ -axes, respectively. On the other hand, the CdI<sub>2</sub>-type layer is only compressed parallel to the  $b$ -axis and is not practically undeformed parallel to the  $a$ -axis. As a result, two different strain fields reside in the RS blocks and CdI<sub>2</sub>-type layers.

The average  $a$ - and  $b_2$ -axes lengths and natural bond lengths, which are expected from the ionic radii, are shown in Table 4. In sample B, those values are 4.84 Å and 4.80 Å, respectively. It is pointed out that the average values of the  $a$ - and  $b_2$ -axis lengths are nearly equal to the natural  $M-O-M$  bond length. Although the length of  $a$ -axis,  $a = 4.90$  Å, is longer than that in the Co-121 phase[17] in which  $a = 4.83$  Å, the  $a$ -axis length is not sufficiently long to release the residual stress for the RS-type blocks, since the natural bond length is in the range of 5.02 Å to 5.075 Å. On the other hand, CdI<sub>2</sub>-type layers are slightly compressed parallel to the  $b$ -direction, namely, the  $b_1$  length of this crystal,  $b_1 = 2.79$  Å, is shorter than that in the Co-121 phase with  $b_1 = 2.82$  Å.

It is conceivable that the strain-type of the present system is influenced by the  $e_{33}$  component, i.e., the strain parallel to the  $c$ -axis. The  $c$ -length of  $[(Bi_{1.84}Co_{0.16})Ca_{2.00}O_y]_{0.58}[CoO_2]$ , 14.36 Å, is

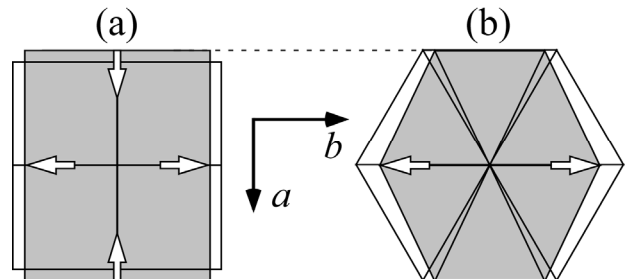


Fig.7 Schematic representation of the  $a$ - $b$  real lattice planes. (a) Distortion-types of the RS-type blocks. (b) corresponding ones of the hexagonal CdI<sub>2</sub>-type layers. Open rectangles and hexagons represent pre-deformed RS-type and CdI<sub>2</sub>-type layers, respectively. Shaded rectangles and hexagons represent deformed RS-type blocks and CdI<sub>2</sub>-type layers, respectively. Arrows with a black edge show the direction of the stress.

**Table 4** Averaged lengths of  $a$ - and  $b_2$ -axes and natural bond lengths of  $M\text{-}O\text{-}M$ .

	Averaged length ( $a + b_2$ )/2 (Å)	Natural bond length of $M\text{-}O\text{-}M$ (Å)
$[(\text{Bi}_{1.84}\text{Co}_{0.16})\text{Ca}_{2.00}\text{O}_y]_{0.58}[\text{CoO}_2]$	4.840	4.80
$[\text{Bi}_{1.94}\text{Ba}_{1.83}\text{O}_y]_{0.56}[\text{RhO}_2]$	5.415	5.42
$[\text{Bi}_{1.79}\text{Sr}_{1.98}\text{O}_y]_{0.63}[\text{RhO}_2]$	5.080	5.02
$[\text{Bi}_{2.08}\text{Sr}_{1.67}\text{O}_y]_{0.54}[\text{CoO}_2]$	5.075	5.02

significantly shorter than that of  $[\text{Bi}_{2.08}\text{Sr}_{1.67}\text{O}_y]_{0.54}[\text{CoO}_2]$  with  $c = 15.25 \text{ \AA}$ . It is, thus, suggested that the 3D-stress resides in the RS-type blocks as well as CdI<sub>2</sub>-type layers in the present system. It is natural to assume that the observed stripe patterns in Fig.5(a) and Fig.6 are a sign of a relaxation mechanism of the stress.

Nearly two-dimensional modulation (local shear-type structural deformation) in the  $a\text{-}b$  plane has been also observed with local discontinuity, i.e., a type of discommensuration in the  $a\text{-}b$  plane. At the same time, some residual strain is expected parallel to the  $c$ -axis. Such shear deformations, i.e., local strain relaxation modes, are frequently observed during the martensitic transformation[26]. During the transformation, homogeneous nucleation-and-growth process causes some rotation of transformed crystals, i.e., the variants. Then, slipping, buckling and twinning deformations are introduced, being at about 45° relative to the compressive and/or tensile transformation strain directions. The martensitic transformation-like structural change from tetragonal-type to orthorhombic-type during the cooling after the synthesis could occur in the present compounds. The domain structures having four different directions, indicated in Fig.6, are a sign of *invariant plane strains*, i.e., martensite-type rotations.

#### 4. Conclusions

We have studied the modulated structure of  $\text{Bi}_{1.84}\text{Ca}_{2.00}\text{Co}_{1.88}\text{O}_x$  based on the electron diffraction and high-resolution microscopy and found that this crystal has a misfit-layered structure, having the chemical formula of  $[(\text{Bi}_{1.84}\text{Co}_{0.16})\text{Ca}_{2.00}\text{O}_y]_{0.58}[\text{CoO}_2]$ . This crystal has a two-dimensionally modulated structure with two modulation vectors,  $\mathbf{q}_1 = -\mathbf{a}^* + 0.58\mathbf{b}_1^*$ ,  $\mathbf{q}_2 = 0.18\mathbf{b}_1^* + 0.5\mathbf{c}^*$ . Curving and fluctuating features of the two subsystems, i.e., the RS-type and the CdI<sub>2</sub>-type layers, are directly observed along  $a$ - and  $c$ -axes, respectively. An important point to emphasize is that present compound has locally domain structure-type modulation in the  $a\text{-}b$  plane.

#### Acknowledgements

This study was partly supported by the Core Research for Evolution Science and Technology (CREST) Project of Japan Science and Technology Agency (JST) and also by a Grant-in-Aid for Scientific Research from the Ministry of Education, Culture, Sports, Science and Technology of Japan.

#### References

- 1) T. Itoh, I. Terasaki, *Jpn. J. Appl. Phys.*, **2000**, *39*, 6658.
- 2) R. Funahashi, I. Matsubara, S. Sodeoka, *Appl. Phys. Lett.*, **2000**, *76*, 2385.
- 3) W. Shin, N. Murayama, *J. Mater. Res.*, **2000**, *15*, 382.
- 4) T. Yamamoto, I. Tsukada, K. Uchinokura, M. Takagi, T. Tsubone, M. Ichihara, K. Kobayashi, *Jpn. J. Appl. Phys.*, **2000**, *39*, L747.
- 5) R. Funahashi, I. Matsubara, *Appl. Phys. Lett.*, **2001**, *79*, 362.
- 6) G. Xu, R. Funahashi, M. Shikano, I. Matsubara, Y. Zhou, *J. Appl. Phys.*, **2002**, *91*, 4344.
- 7) H. Leligny, D. Grebille, O. Pérez, A. C. Masset, M. Hervieu, C. Michel, B. Raveau, *C. R. Acad. Sci. Paris Série IIc*, **1999**, *2*, 409.
- 8) H. Leligny, D. Grebille, O. Pérez, A. C. Masset, M. Hervieu, B. Raveau, *Acta Crystallogr. B*, **2000**, *56*, 173.
- 9) A. Maignan, S. Hébert, M. Hervieu, C. Michel, D. Pelloquin, D. Khomskii, *J. Phys.: Condens. Matter*, **2003**, *15*, 2711.
- 10) E. Guilemau, M. Mikami, R. Funahashi, D. Chateigner, *J. Mater. Res.*, **2005**, *20*, 1002.
- 11) D. Grebille, H. Muguerza, O. Pérez, E. Guilmeau, H. Rousselière, R. Funahashi, *Acta Crystallogr. B*, **2007**, *63*, 373.
- 12) E. Guilmeau, M. Pollet, D. Grebille, M. Hervieu, H. Muguerza, R. Cloots, M. Mikami, R. Funahashi, *Inorg. Chem.*, **2007**, *46*, 2124.
- 13) M. Hervieu, A. Maignan, C. Michel, V. Hardy, N. Créon, B. Raveau, *Phys. Rev. B*, **2003**, *67*, 045112.
- 14) K. Yubuta, S. Okada, Y. Miyazaki, I. Terasaki, T. Kajitani, *Jpn. J. Appl. Phys.*, **2006**, *45*, 179.
- 15) K. Yubuta, S. Begum, Y. Ono, Y. Miyazaki, T. Kajitani, *Jpn. J. Appl. Phys.*, **2006**, *45*, 4159.
- 16) K. Yubuta, S. Okada, Y. Miyazaki, I. Terasaki, T. Kajitani, *Jpn. J. Appl. Phys.*, **2005**, *44*, 8557.
- 17) Y. Miyazaki, M. Onoda, T. Oku, M. Kikuchi, Y. Ishi, Y. Ono, Y. Morii, T. Kajitani, *J. Phys. Soc. Jpn.*, **2002**, *71*, 491.
- 18) Y. Miyazaki, T. Miura, M. Onoda, M. Uchida, Y. Ishii, Y. Ono, Y. Morii, T. Kajitani, *Jpn. J. Appl. Phys.*, **2003**, *42*, 7467.
- 19) *International Tables for Crystallography Vol. A*, ed. T. Hahn, Kluwer, Dordrecht, **2002**.
- 20) J.-M. Tarascon, R. Ramesh, P. Barboux, M. S. Hedge, G. W. Hull, L. H. Greene, M. Giroud, Y. LePage, W. R. McKinnon, J. V. Waszczak, L. F. Schneemeyer, *Solid State Commun.*, **1989**, *71*, 663.
- 21) Y. Matsui, H. Maeda, Y. Tanaka, S. Horiuchi, *Jpn. J. Appl. Phys.*, **1988**, *27*, L372.
- 22) H. W. Zandbergen, W. A. Groen, A. Smit, G. van Tendeloo, *Physica C*, **1990**, *168*, 426.
- 23) O. Ebil, *Physica C*, **1990**, *168*, 215.
- 24) K. Yanagisawa, Y. Matsui, K. Shoda, E. Takayama-Muromachi, S. Horiuchi, *Physica C*, **1992**, *196*, 34.
- 25) D. Pelloquin, A. C. Masset, A. Maignan, M. Hervieu, C. Michel, B. Raveau, *J. Solid. State. Chem.*, **1999**, *148*, 108.
- 26) Z. Nishiyama, *Martensitic Transformation*, ed. M. E. Fine, M. Meshii, C. M. Wayman, Academic Press, New York, **1978**.